26th EPS Conf. on Contr. Fusion and Plasma Physics, Maastricht, 14 - 18 June 1999 ECA Vol.23J (1999) 17 - 20

PHYSICS OPTIMIZATION OF A QUASI-OMNIGENEOUS STELLARATOR*

J.F. Lyon, S.P. Hirshman, D.A. Spong, R. Sanchez, L.A. Berry, J.C. Whitson, D.B. Batchelor, J. Carlsson, B.E. Nelson

Oak Ridge National Laboratory, Oak Ridge TN 38731-8072, U.S.A.

Compact Stellarators with plasma aspect ratios $A_p = \langle R \rangle / \langle a \rangle$ = 2-4 are of interest because they may combine the best features of tokamaks (moderate aspect ratio, good confinement and beta) and stellarators (disruption immunity, no current drive, low recirculating power in a reactor). Here $\langle R \rangle$ and $\langle a \rangle$ are the average major and minor radii of the plasma. The benefits of lower A_p are larger plasma size for a given cost for an experiment and lower cost for a given fusion power in a reactor. Two complementary approaches are being studied for Compact Stellarators. Quasi-axisymmetric stellarators [1] have tokamak-like symmetry properties and a bootstrap current comparable to that in a tokamak. The quasi-omnigeneous (QO) stellarators [2] examined here use a spectrum of magnetic field spatial harmonics to minimize the deviation of bounce-averaged drift orbit (approximate second adiabatic invariant J*) surfaces from magnetic surfaces (Fig. 1). The approximate alignment of drift surfaces with flux surfaces reduces energetic orbit losses and neoclassical transport. The low bootstrap current, typically ~1/10 that in a comparable tokamak, should lead to configurations that are relatively insensitive to beta and are robust against current-driven modes (external kinks), vertical instabilities, and disruptions.

1. Quasi-Omnigeneous Stellarator Optimization

Quasi-omnigeneous stellarators have some general similarity to the drift-optimized Wendelstein 7-X (W7-X) "helias" configuration [3] but QO configurations have plasma aspect ratios smaller by a factor of 3-4, a significant bootstrap current, a larger helical component, and a smaller mirror-like variation of the magnetic field on a flux surface. Although the W7-X configuration has very attractive physics properties, it leads to a large ($\langle R \rangle$ = 22 m) reactor. Compact QO configurations are of interest because they could lead to reactors with a volume-average beta $\langle \beta \rangle$ = 4-5% and $\langle R \rangle$ ~ 9 m, closer to the reverse-shear ARIES-RS tokamak reactor in the ratio of reactor mass to generated power.

The optimization criteria for QO configurations are their confinement properties, β limits, and feasibility of the modular coil set. The goals are (1) energy confinement times $\tau_E > 2\tau_E^{ISS95}$, where τ_E^{ISS95} is the empirical stellarator confinement scaling [4]; (2) $\langle \beta \rangle$ ~ 4% (for a reactor); and (3) modular coils with sufficient access for heating and diagnostics. Previously, the iterative optimization loop calculated the shape of the LCFS that produces the desired physics properties using measures of trapped particle confinement (poloidal variation of B_{max}, B_{min}, J*), β limits (global magnetic well, Mercier stability), magnetic field ripple, outer surface curvature, and limits on the total current and rotational transform ι (= 1/q) profiles. Figure 1 shows the type of improvement obtained as a result of the optimization procedure; the flux surfaces are

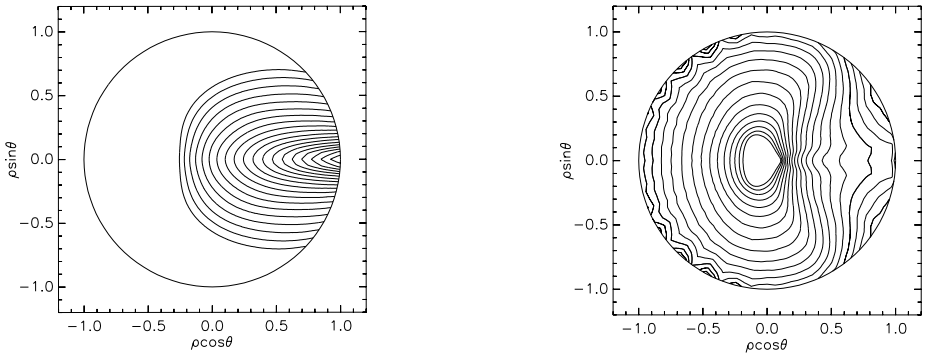

Fig. 1. Open J contours (left) before and closed (right) after the optimization for helically trapped particles.*

concentric circles in this magnetic coordinate system. Similar improvements are obtained for passing particles, but the drift surfaces in the $v_{||}/v$ range where orbits change from helically trapped to passing are not as well confined, and these determine the neoclassical transport.

Different QO configurations are obtained depending on whether one is optimizing for: (1) a reactor (where the critical issues are maximizing the space between the LCFS and the center of the coil winding surface, $\langle\beta\rangle$, and alpha-particle confinement); or (2) for a modest ($\langle R\rangle \sim 1$ m, $B \sim 1$ T, $P < 2$ MW) concept exploration experiment designed to test the physics of the QO approach (where confinement and configuration flexibility are more important issues). We have studied both optimizations, but this paper deals primarily with the experimental optimization.

QO-optimized configurations with toroidal field periods $N_{fp} = 3$ and 4 and A_p from 3 to 4.8 were examined. Figure 2 shows the LCFS for an $N_{fp} = 3$ $A_p = 3.6$ QO configuration optimized for an experiment and the modular coil set that creates it. Additional coils (not shown) are needed for configuration flexibility. The colors indicate contours of constant $|B|$. Figure 3 shows the spatial Fourier spectrum of |B| components for this configuration. The largest components are the helical, axisymmetric "1/R" term (a factor of 4 larger in an equivalent tokamak), and "bumpy" (mirror) terms. The spectrum of smaller compensating field terms is that needed to satisfy the physics constraints at lower aspect ratio. The on-axis field is normalized to 1 on this scale and the rotational transform varies from $\iota_0 = 0.55$ on axis to $\iota_a = 0.64$ at the plasma edge.

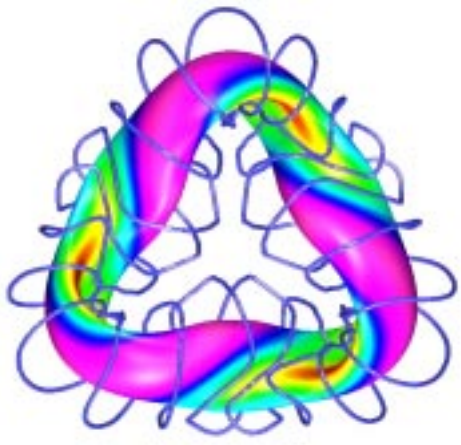

Fig. 2. LCFS and coils for an $N_{fp} = 3$ case.

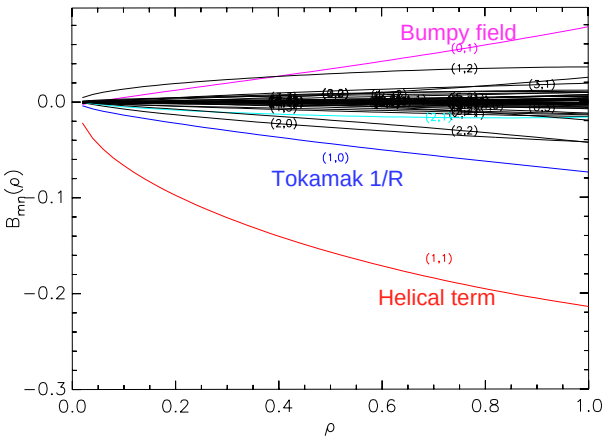

Fig. 3. Magnetic field structure for plasma in Fig. 2.

QO optimization reduces neoclassical transport because cross-field drifts scale with $\langle v_d \bullet \nabla\psi \rangle \propto \partial J^*/\partial\theta$ where v_d is the particle drift velocity, ψ is the flux, and θ is the poloidal angle. Figure 4 shows the result of a Monte Carlo calculation of the particle diffusivity D and heat diffusivity χ for an $N_{fp} = 4$ $A_p = 4.2$ QO configuration. It was obtained by following four groups of test particles with energies 0.5, 1, 2, and 3 keV in a background plasma with 1-keV temperature and 5×10^{19} m^{-3} density with different radial electric fields. The results were integrated over a Maxwellian distribution and the 0-D energy confinement time $\tau_E = \langle a \rangle^2/4\chi$ where χ was obtained from the energy moment in the integration. The values for D and χ decrease with decreasing density (and collisionality ν^*) and do not exhibit the $1/\nu*$ transport scaling normally associated with ripple-induced losses. For comparison, twice the τ_E^{ISS95} is 11.4 ms at P = 2 MW, about the same as the neoclassical value with no ambipolar electric field.

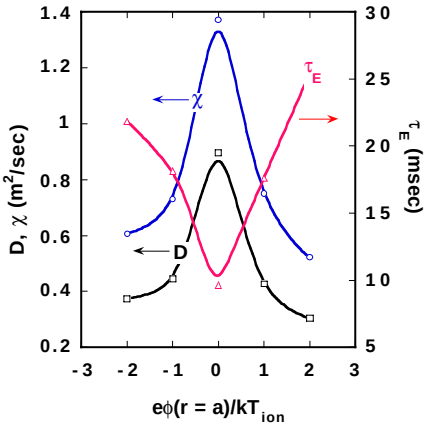

Fig. 4. Dependence of transport on the radial electric field

Energetic orbit confinement is important for heating schemes that rely on these particles in an experiment and for adequate alpha-particle confinement in a reactor. The compatibility of QO configurations with ion cyclotron range of frequency (ICRF) heating has been simulated in two ways. For simulating an experiment with energetic tail ICRF heating, 20-keV ions were launched at their turning points at the field resonance and followed collisionlessly. The loss rates were less than that for the CHS experiment in which ICRF heating was used successfully. Monte Carlo calculations have also started using a quasilinear ICRF diffusion operator to follow particles as they diffuse up in energy, allowing study of fundamental as well as minority tail ICRF heating. Following 500 3.5-MeV alpha particles for a reactor-scale version indicates an energy loss rate of ~20%, which is marginally acceptable for this application.

2. Optimization Improvement

The development in the last year of much improved QO configurations with a stronger physics basis is due to incorporation of much faster (factor ~10) calculations of both the self-consistent bootstrap current and the ballooning stability limit within the iterative optimization loop. The fast 3-D bootstrap code (BOOTSJ) has allowed determination of QO configurations with self-consistent bootstrap current. Figure 5 shows the radial variation of the bootstrap current from BOOTSJ and VMEC [5] equilibrium solver that computes the magnetic field, metric elements, and other relevant surface quantities for a modified N_{fp} = 3 A_p = 3.6 QO configuration that is ballooning and Mercier stable at $\langle\beta\rangle$ = 2%. The bootstrap current is 19 kA for the assumed density and temperature profiles. This is much smaller than the 380-kA plasma current in a tokamak with equivalent cross section and rotational transform. The current is not in the direction to stabilize neoclassical islands and tearing modes, but is thought to be sufficiently small to have little effect. Stability against external kinks or vertical instability is also expected for the same reason, but calculations are underway to check this.

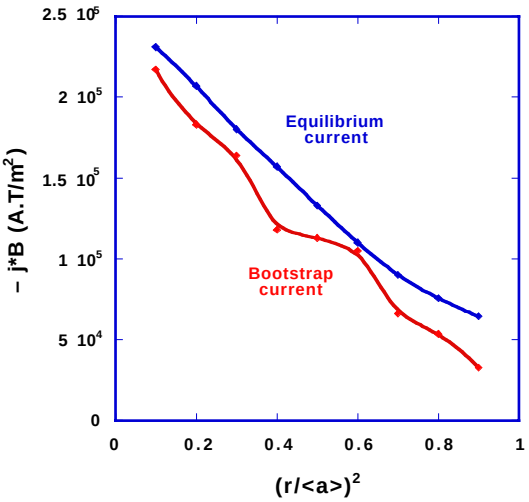

Fig. 5. QO bootstrap current profiles.

QO configurations are relatively insensitive to changes in $\langle\beta\rangle$. Figure 5 shows the plasma cross sections at the beginning, 1/4, and 1/2 way through a field period for $\langle\beta\rangle$ = 0 and 6%. There is little outward shift of the magnetic axis; the small bootstrap current produces only a small (~10%) change in $\iota(r)$.

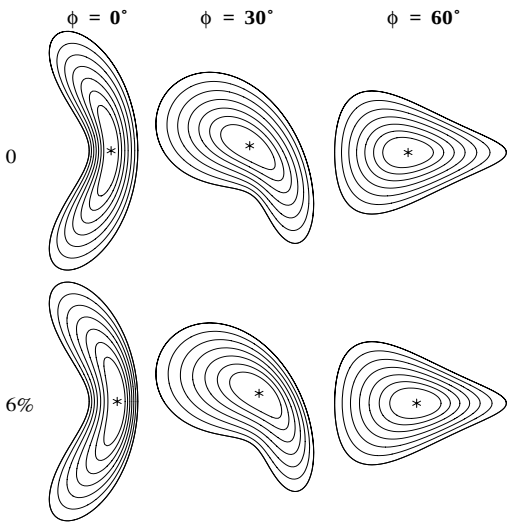

Fig. 6. Insensitivity of the plasma to increasing beta.

Although the modest concept-exploration-level experiment discussed thus far would be power limited to $\langle\beta\rangle$ < 2%, higher values of beta ($\langle\beta\rangle$ > 4%) are needed for an attractive reactor. Ideal ballooning modes set the critical $\langle\beta\rangle$ for QO stellarators rather than kink modes because the bootstrap current is rather small, typically ~ a few tens of kA. Ballooning instabilities are local modes that are driven unstable by the presence of pressure gradients in regions of bad local curvature. Their stabilization is difficult because their behavior is governed by local quantities like the local shear or the local curvature. The fast 3-D ideal ballooning code

COBRA [6] has been developed to evaluate the ballooning growth rate on a prescribed set of flux surfaces and initial points for a given equilibrium. Integration of COBRA into the configuration optimization code has resulted in configurations with twice the value of $\langle\beta\rangle$ while preserving good transport properties. Figure 7 shows how the $N_{fp} = 3$ $A_p = 3.6$ QO configuration in Fig. 2 was modified to be stable at $\langle\beta\rangle = 3\%$. Figure 8 shows the modification of the original (unstable) configuration to the final (stable) configuration in the vertically elongated cross section. The rotational transform profile also changed at $\langle\beta\rangle = 3\%$ from nonmonotonic to monotonically increasing with radius. Small changes in the pressure profile used in Fig. 7 gave ballooning stability at $\langle\beta\rangle > 4\%$ for this final configuration. Newer configurations with higher rotational transform ($\iota_0 = 0.78$, $\iota_a = 0.91$) are also ballooning stable at $\langle\beta\rangle = 4\%$ with good confinement and small self-consistent bootstrap current. Earlier reactor-scale QO configurations had $\langle\beta\rangle$ up to ≈7%, good confinement, and a low bootstrap current contribution to ι, but the bootstrap current in those cases was not self-consistent with the MHD equilibrium.

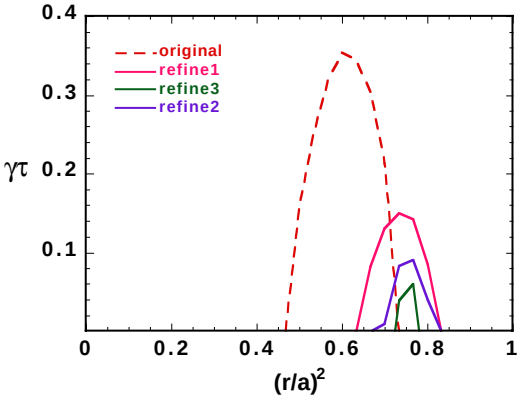

Fig. 7. Reduction of ballooning growth rate at $\langle\beta\rangle = 3\%$.

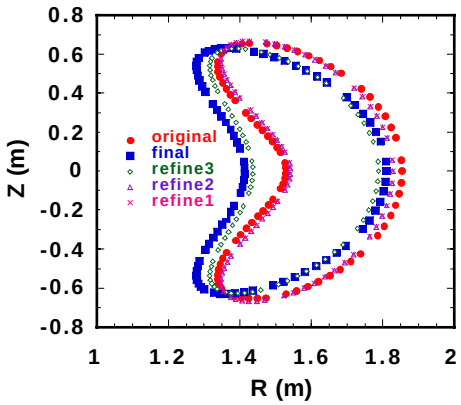

Fig. 8. Surface changes corresponding to Fig. 7.

Two improved measures of confinement are planned in the QO configuration optimization code. The approximate adiabatic invariant J* (calculated by integrating $v_{||}$ along the toroidal angle in magnetic coordinates) will be replaced by the more accurate second adiabatic invariant J (calculated by integrating $v_{||}$ along the magnetic field) and extended to passing particles for a better calculation of orbit losses. A measure of local diffusive transport will be calculated in the optimization loop with the DKES (drift kinetic equation solver) code [7].

Nonplanar modular coils that accurately create the desired LCFS with adequate distances between the plasma and the coils, and between adjacent coils for heating and diagnostic access, (Fig. 2) were found by iteratively varying the parameters describing the coils until the desired match with the LCFS was obtained. The next step in improving the coil optimization code is to add constraints on the minimum bend radius and the distance between coils for finite cross section coils. The distance between the LCFS and the center of the coil winding surface and the ratio of B_{max} on the coils to B_0 on axis will be optimized for studying the reactor extrapolation.

References

[1] A. Reiman et al., IAEA-F1-CN-69/ICP/06, Proc. 17th IAEA Conf., Yokohama (1998).
[2] D.A. Spong et al., IAEA-F1-CN-69/ICP/07, Proc. 17th IAEA Conf., Yokohama (1998).
[3] J. Nührenberg and R. Zille, Phys. Lett. A 129, 1139 (1988).
[4] U. Stroth et al., *Nucl. Fusion* **36**, 1063 (1996).
[5] S.P. Hirshman and J.C. Whitson, *Phys. Fluids* **26**, 3553 (1983).
[6] R. Sanchez et al, submitted to *J. Comp. Phys.* (1999).
[7] S.P. Hirshman and W.I. van Rij, *Phys. Fluids B* **1**, 563 (1989).

* Research supported by the USDOE under contract DE-AC05-96OR22464 with Lockheed Martin Energy Research Corp.